Impact of cool-down conditions at T_c on the superconducting rf cavity quality factor

J.-M. Vogt,* O. Kugeler, and J. Knobloch
Helmholtz-Zentrum Berlin, Germany
(Received 8 July 2013; published 9 October 2013)

Many next-generation, high-gradient accelerator applications, from energy-recovery linacs to accelerator-driven systems (ADS) rely on continuous wave (CW) operation for which superconducting radio-frequency (SRF) systems are the enabling technology. However, while SRF cavities dissipate little power, they must be cooled by liquid helium and for many CW accelerators the complexity as well as the investment and operating costs of the cryoplant can prove to be prohibitive. We investigated ways to reduce the dynamic losses by improving the residual resistance (R_{res}) of niobium cavities. Both the material treatment and the magnetic shielding are known to have an impact. In addition, we found that R_{res} can be reduced significantly when the cool-down conditions during the superconducting phase transition of the niobium are optimized. We believe that not only do the cool-down conditions impact the level to which external magnetic flux is trapped in the cavity but also that thermoelectric currents are generated which in turn create additional flux that can be trapped. Therefore, we investigated the generation of flux and the dynamics of flux trapping and release in a simple model niobium-titanium system that mimics an SRF cavity in its helium tank. We indeed found that thermal gradients along the system during the superconducting transition can generate a thermoelectric current and magnetic flux, which subsequently can be trapped. These effects may explain the observed variation of the cavity's R_{res} with cool-down conditions.

DOI: 10.1103/PhysRevSTAB.16.102002 PACS numbers: 29.20.−c, 74.25.Ha, 74.25.Wx

I. INTRODUCTION

Next-generation accelerator applications frequently demand high-field continuous wave (CW) operation based on superconducting radio-frequency (SRF) systems. Unlike for pulsed systems, a whole new set of challenges must therefore be addressed. At the forefront is the requirement that their dynamic losses must be drastically reduced.

The losses in SRF cavities are determined by the surface resistance R_s which consists of a temperature-dependent contribution given by BCS theory R_{BCS} and a residual term R_{res}:

$$R_s = R_{\mathrm{BCS}} + R_{\mathrm{res}}. \quad (1)$$

While R_{BCS} can be lowered by reducing the cavity's operating temperature we studied measures to manipulate R_{res} in TESLA-type cavities. The commonly known strategy towards an improved cavity performance is a combination of surface treatments and bakeouts [1]. They improve the surface smoothness, eliminate field emitters, and prevent Q disease, i.e., hydrogen diffusion from the bulk to the cavity surface forming hydrides which results in an increased R_{res} [2]. Processing steps for TESLA-type cavities are listed in Ref. [3]. Typically obtained R_{res} values are of the order of 10 nΩ at 1.8 K which is above the BCS limit of 4.4 nΩ at this temperature. The BCS limit can only be approached when every source of R_{res} degradation is addressed.

In our work we focus on the contribution of trapped magnetic flux and its dynamics. Studies have shown that the Meissner effect in the niobium which is used for SRF cavity fabrication is incomplete due to imperfections of the crystal lattice such as impurities, dislocations, and grain boundaries which pin up to 100% of the magnetic flux lines [4,5]. The result is a significant increase in R_{res} that scales linear with the amount of trapped flux. For the normal-conducting areas at the center of each flux tube, the skin effect comes into effect thus the surface resistance scales with the square root of the operating frequency. Detailed calculations for the dissipated power due to trapped vortices include additional parameter as the density of trapped flux lines and the location of the pinning centers [6]. An increase in R_{res} of 3.5 nΩ for every trapped μT was experimentally determined for a 1.3 GHz niobium cavity [3].

During normal operation, TESLA-type cavities typically achieve surface resistances of about 10 nΩ. It is obvious that any external magnetic field must be avoided to achieve this goal. Therefore, magnetic shielding around the cavity reduces the earth's magnetic field (55 μT) down to a level of 1 μT. However, almost all shielded cavities are operated far from the BCS limit due to additional R_{res} contributions.

*julia.vogt@helmholtz-berlin.de

Our experiments show that we are able to manipulate R_{res} by adapting the cool-down conditions of a cavity. One possible cause is that shielding alone is not sufficient to eliminate R_{res} because additional magnetic flux due to thermoelectric currents is generated inside the cavity during the cooldown that then gets trapped in the cavity walls. The detailed correlation of cool-down parameters and obtained R_{res} is given in this paper. Furthermore, the dynamics of flux pinning, trapping, and expulsion during superconducting phase transition impact R_{res}. These mechanisms have been studied extensively in the mixed state of type II superconductors but the related effect in the Meissner regime is not fully understood yet. In addition to cavity measurements, we designed a model system that made it easier to study these aspects in detail.

II. THERMAL CYCLING OF A TESLA CAVITY

A. Experiment

We investigated the surface resistance of fully dressed TESLA-type SRF cavities that were cooled down to the operating temperature (1.8 K) under different conditions, in particular different temperature distributions along the cavity axis during superconducting phase transition.

All test were performed in the HoBiCaT horizontal test facility setup [7] with double magnetic shielding (one cold and one warm). The residual field seen by the cavity was of the order of 0.3 μT. Thus, in theory, a residual resistance of 1 nΩ should be achievable. A TTF-III coupler very near critical coupling (β values between 1 and 2) was employed. The temperature of the cavity was monitored by three Cernox sensors. Figure 1 indicates the positions at which the sensors were placed and the position of helium tank and inlet.

The cooldown from room temperature was performed quickly to avoid the Q disease in the temperature range 50–150 K. In an earlier experiment, we were able to demonstrate that a thermal cycling procedure after the cooldown can be utilized to reduce a cavity's residual resistance [8]. In a thermal cycle, the cavity is warmed briefly above the transition temperature of 9.2 K and cooled down again. The measurements presented here reproduced the effect and a reduction of R_{res} by a factor of 2.5 was achieved.

Figure 2 displays the obtained R_s values for the cool-down from room temperature and for four different thermal

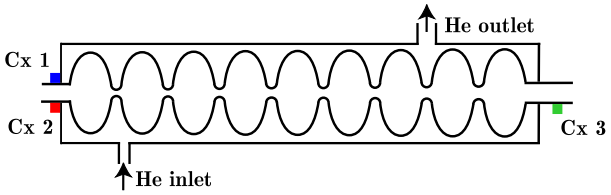

FIG. 1. Cavity welded into a helium tank with the positions of the Cernox sensors (Cx) and the helium inlet and outlet.

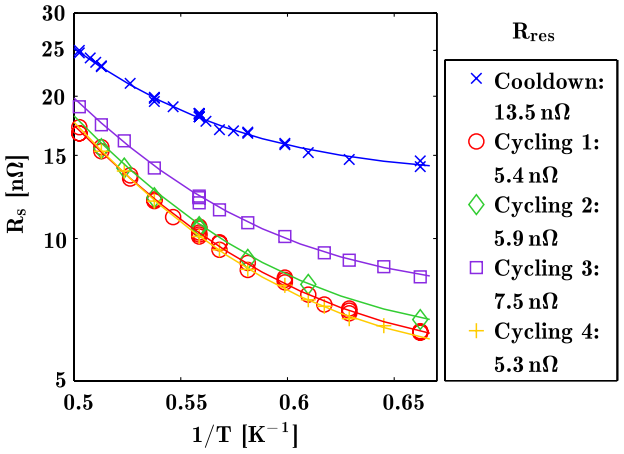

FIG. 2. Surface resistance versus cavity temperature at 4 MV/m gradient. Error bars are within the symbol size. The colored lines represent the fit to the data points.

cycles measured at an accelerating gradient of $E_{acc} = 4$ MV/m versus the liquid helium bath temperature. The uppermost curve (×) shows R_s after the initial cooldown. During the cooldown, very large temperature gradients existed along the cavity when it went superconducting (see Fig. 3). The temperature dependence of R_s can be described semiempirically [9]:

$$R_s(T) = \left(\frac{A}{T}\right)\exp\left(-\frac{B}{T}\right) + R_{res} \qquad (2)$$

with $A, B \approx 1.9T_c$ and R_{res} as fitting parameters. Thereby, we determined a temperature-independent residual resistance of 13.5 nΩ after the cooldown.

In a first cycling procedure following the initial cooldown, the helium supply was turned off and the cavity was given just enough time to make the transition to normal conduction which was determined by monitoring

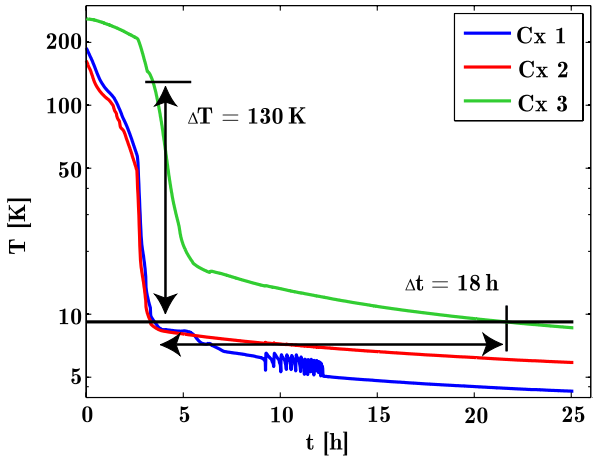

FIG. 3. Temperatures at different positions along the cavity (see Fig. 1) during cooldown from room temperature. The horizontal black line indicates the transition temperature of 9.2 K. The definitions for ΔT and Δt used in the text are marked in the plot.

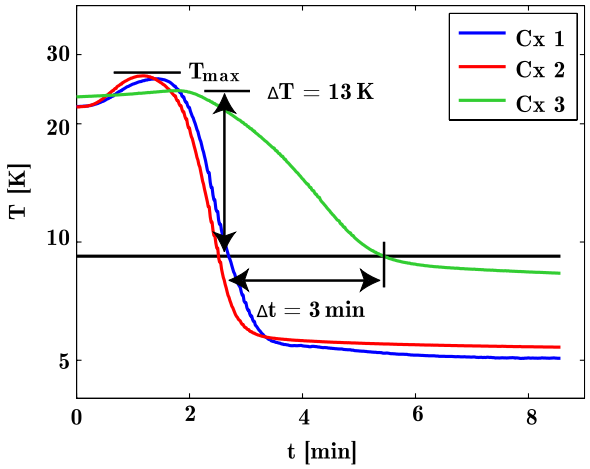

FIG. 4. Temperatures at different positions along the cavity (see Fig. 1) during thermal cycle 1. The horizontal black line indicates the transition temperature of 9.2 K.

the temperature of the outgoing helium gas. Then, helium supply and vacuum pumps were turned on again. As a result, the temperature gradients were reduced significantly compared to the initial cooldown (see Fig. 4). The resulting R_{res} value went down to 5.4 nΩ ($\circ$). In subsequent cycling runs it was attempted to increase R_{res} again by turning off the cryoplant for a longer time. The second cycle ($\diamond$) gave a small reduction in R_{res} down to 5.9 nΩ which, however, was not significant. Therefore, cycling was repeated with four hours of cryo-downtime in this particular case and a significantly increased residual resistance to 7.5 nΩ could be demonstrated ($\square$). Since the monitored temperatures went beyond the 50 K limit, one might argue that the increase in resistance could have been caused by Q disease. A fourth cycling procedure with an even shorter cryo-downtime ($+$) was thus used to improve R_{res} again. With 5.3 nΩ, this result was even better than the previous values. All obtained R_{res} values and benchmark data for the respective cycle are assembled in Table I. The error bars of the stated R_{res} values arise out of the accuracy of the rf measurements which is below 10%. The fits using Eq. (2) yielded a constant BCS contribution for all performed measurements ($A \approx 1.8 \times 10^{-4}$ Ω K, $B \approx 17.8$ K).

TABLE I. Parameters of cooldown and the performed thermal cycles: maximum temperature reached by the cavity T_{max}, temperature difference along the cavity during superconducting phase transition ΔT, duration of the phase transition Δt, and residual resistance after the respective procedure R_{res}.

	R_{res} [nΩ]	T_{max} [K]	ΔT [K]	Δt
Cooldown	13.5	300	130	18 h
Cycling 1	5.4	26	13	3 min
Cycling 2	5.9	42	32	10 min
Cycling 3	7.5	52	42	13 min
Cycling 4	5.3	23	5	1 min

A similar improvement of R_{res} upon thermal cycling was observed in earlier experiments utilizing a different TESLA-type cavity [8]. There, an initial residual resistance of 10.8 nΩ was measured. Thermal cycling reduced R_{res} to 3.6 nΩ and a variation of cycling parameters led to a variation of R_{res} in the range of 3.6–6.6 nΩ. The data is consistent with the values presented here.

B. Discussion

We can conceive various explanations for the R_{res} improvement upon thermal cycling. Since all measurements were performed on the very same cavity in the same measurement run, most properties which impact R_{res}, like residual-resistance ratio (RRR), granularity, surface morphology, etc. are unchanged thus reducing the possible explanations. We discuss the most likely candidates in the following sections.

1. Changes in surface contaminants after first cycle

One explanation is the variation in condensed surface contaminants. They degas during the period of increased cavity temperature and migrate towards less harmful areas. This hypothesis however cannot explain the fact that R_{res} was increased by the third cycle, the one with the longest duration and the highest temperatures and gradients. One might argue that the increased temperatures caused Q disease. However, Q disease is irreversible below 150 K. Hence, the fourth cycle which restored the low R_{res} value contradicts this explanation.

We thus discarded the hypothesis that surface contaminants were responsible for the observed R_{res} improvement and concentrated on trapped magnetic flux. Here, different effects may play a role. These include changes in the efficacy of the magnetic shielding depending on the temperature of the shield at the time of the superconducting phase transition, changes in the flux expulsion ability (more complete Meissner effect) or changes in the local ambient magnetic field that may result from thermoelectric currents.

2. Efficacy of the magnetic shielding

The level of ambient field at the cavity is defined by the magnetic shielding and its efficacy. Being separated from the cavity by a superinsulation, the inner magnetic shielding cools down slower than the cavity itself. Since the permeability quoted by the manufacturer (Cryoperm) is temperature dependent [8], the effective ambient magnetic field at the cavity at superconducting phase transition may depend on the cool-down history. During the initial cooldown the shield temperature is typically of the order of 150 K at the superconducting phase transition, while the optimal shielding is quoted to be at 4 K.

However, in fact permeability measurements of the utilized magnetic shielding materials versus temperature yielded no significant temperature dependence at the relevant temperatures [8]. We even observed a small

decrease of permeability towards lower temperatures which should, if anything, lead to a larger R_{res} after the first cycle instead of the observed reduction. Also, measurements of the shield temperature yielded no correlation to the obtained R_{res}.

3. Thermal currents

Since the magnetic shielding from external field appears unaffected by the cool-down history, the generation of additional field within the shielding must be considered.

A magnetic field could be generated by the thermoelectric effect. As mentioned above, the cool-down procedure of a cavity is optimized to avoid Q disease by passing through the temperature range (50–150 K) as quick as possible leading to large temperature gradient along the cavity because the helium inlet is positioned off center. Figure 3 displays the temperatures near the phase transition. While both ends of the cavity are at different temperatures, the cavity-tank-system forms a thermocouple (see Fig. 5). Niobium cavity and titanium tank have different charge carrier velocities thus a thermal voltage is induced:

$$V = (S_{Nb} - S_{Ti}) \cdot (T_1 - T_2), \tag{3}$$

where S_{Nb} and S_{Ti} are the thermopowers of the respective material. There are only a few measurements of these parameters at cryogenic temperatures available. Furthermore they are contradictory. We measured the effective (temperature-dependent) thermopower $(S_{Nb} - S_{Ti})$ to be of the order of 1 μV/K at 10 K [10]. $T_{1,2}$ are the temperatures of the two contact points between tank and cavity. Given the measured temperature differences we expect induced voltages of the order of 130 μV for the cooldown and 5–50 μV for the thermoelectric cycles.

The thermal voltage drives a thermal current because the cavity is welded into the tank and hence we have a closed loop. The current flows along the cavity walls in the axial direction and back through the titanium tank. It generates a magnetic field that cannot be screened by the magnetic shielding since it originates from within it. Since the resistance of the helium tank is well below 1 mΩ, even thermoelectric voltages less than 1 mV will generate strong currents. The Ohmic resistivity of titanium at 10 K is of the order of 100 nΩ m [11]. Hence, for the titanium tank the resistance evaluates to approximately 100 $\mu\Omega$. With the thermopower $(S_{Nb} - S_{Ti})$ of about 1 μV/K and

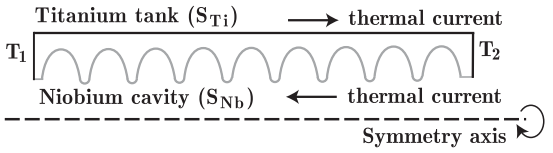

FIG. 5. Thermocouple formed by helium tank (Ti) and cavity (Nb). The direction of current is given by the signs of $(T_1 - T_2)$ and $(S_{Nb} - S_{Ti})$.

temperature differences as stated in Table I, we expect a current in the 1 A range for the initial cooldown and in the 1/10 A range for a cycle. A line current of 1 A will generate a field of 2 μT at a radius of 10 cm, which is roughly the size of the cavity. Thus, it is conceivable that magnetic fields well into the μT range can be generated along the length of the cavity.

In the instance of the superconducting phase transition, the flux may be partially trapped in the cavity walls. Note that once the niobium is superconducting its contribution to the thermopower drops to zero, nevertheless the contribution of the titanium tank remains. Hence, the measured variation in trapped flux of several μT may realistically be generated by thermocurrent.

Figure 6 displays the temperature difference ΔT between both contact points of cavity and tank at the onset of phase transition compared to the surface resistance measured after the respective cycle. The onset of phase transition was defined as the instance when the first temperature sensor at the positions indicated in Fig. 1 dropped below transition temperature. Here, the temperature difference ΔT between the sensors was calculated as indicated in Figs. 3 and 4. Figure 6 suggests that a large ΔT is correlated with an increased R_{res} and a decreased ΔT leads to a reduced R_{res}. The data is a strong indication that thermal currents contribute to R_{res} and hence a possible explanation for the cycling effect. Nevertheless one more factor, the duration of the phase transition, must be evaluated.

4. Transition duration

Not only does ΔT vary from cycle to cycle but also the duration of the cavity's phase transition Δt depends on the cooling history. Ambient magnetic flux starts to be trapped when the first regions of the cavity pass into the

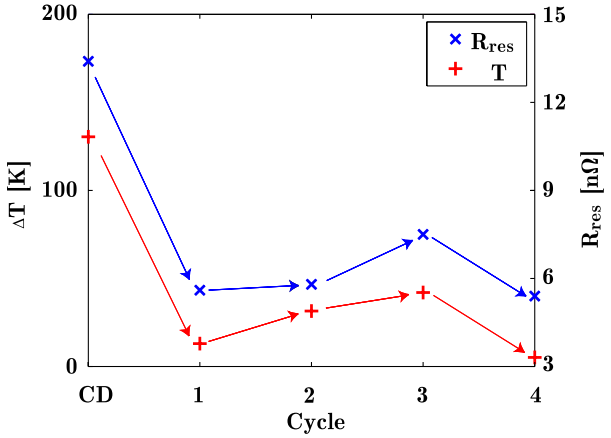

FIG. 6. Temperature difference along the cavity at the onset of the superconducting phase transition (ΔT) and residual resistance (R_{res}) measured in the superconducting state for the cooldown (CD) and for four thermal cycles. The onset of phase transition was defined as the instance when the first temperature sensor at the cavity dropped below the transition temperature.

superconducting state and the process is ongoing until the whole cavity is superconducting. So far, the trapping dynamics during this time are unknown though it seems likely that the duration of the phase transition process influences the amount of trapped flux in the cavity.

Unfortunately, in our setup Δt is strongly correlated with the temperature difference ΔT as listed in Table I. Both the transition duration and the thermal gradients are small for a short cycle (cycle 1 or 4). A long cycle automatically generates large thermal gradients. Hence, the results presented here do not allow us to make conclusive statements on the effect of Δt on R_{res}. We are in the process of modifying the thermal cycle to separate out this effect as well.

The presented results imply that the quality factor of SRF cavities is influenced by temperature gradients and the flux trapping behavior of the used material. The explicit mechanisms cannot be understood by cavity investigations because the setup is too complex for precisely controlled experiments. We need to simplify the geometry and to add more diagnostic equipment to understand the niobium material properties. On the other hand, rf measurements are not mandatory because we want to investigate the basics of flux trapping dynamics in niobium independently from the cavity application. The next section will explain a model system that we developed for these studies.

III. EXPERIMENTS ON MODEL SYSTEM

A. Setup

The change in R_{res} observed in SRF cavities may be explained by a variation of trapped magnetic flux. The changed level of flux may originate from the thermoelectric effect which is based on basic material properties. Hence, we developed a model system resembling the materials and their configuration in a dressed cavity.

The setup for the model experiments shown in Fig. 7 is based on a 30 cm long RRR 300 niobium rod (square cross section of 84×84 mm^2). It was anchored to a 4.2 K helium reservoir at both ends and equipped with two separately operable, resistive heaters (one on each end) for imposing spatial temperature gradients and varying the cool-down rate. The temperature distribution was monitored with seven Cernox sensors. Five were attached along the rod axis and one close to each heater. In order to simulate the conditions in a cavity-tank system, both rod ends were shorted out with a grade 2 titanium rod forming a thermal and electrical circuit. Thereby thermoelectric properties of the niobium-titanium system close to transition temperature were measured. Magnetic flux densities were observed by placing a 3D fluxgate magnetometer (FM) near the center of the rod. Each FM (6 mm diameter and 32 mm length) consisted of a plastic coating and a thin, very soft ferromagnetic core with a low remanence (1 mm diameter, 26 mm length) [12,13].

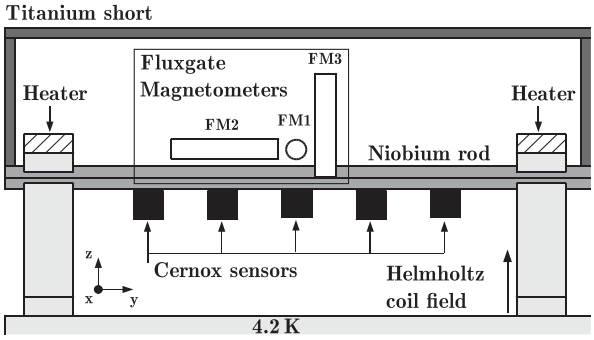

FIG. 7. Experimental setup of the cavity-tank "model" and position of instruments.

The whole construction was placed inside HoBiCaT where an ambient field of about 3 μT was measured (without cold shielding). A Helmholtz coil (HC) was placed around the setup and used to generate an additional field in the z direction. Alternatively, the HC could be removed and a second magnetic shielding was placed around the setup, reducing the ambient field below 50 nT.

B. Results

1. Thermal currents

First, we investigated the thermoelectric effect in the niobium-titanium system and its consequences concerning generation and trapping of magnetic flux.

Here, we used the second magnetic shielding for reduction of any ambient field. The heaters were employed to bring the two contact points of niobium and titanium to different temperatures. We measured the thermoelectric properties and the induced magnetic fields. We were able to resolve a number of issues: (i) Thermally induced currents do exist in the niobium-titanium system near T_c and they create a magnetic field. The field is similar to the one induced by an externally applied electric current. This was verified by opening the loop and attaching a current source to the niobium rod instead of the titanium short circuit. The electrical current was adjusted until it resulted in the same magnetic field value as the thermal current. The required electrical currents were in the mA range consistent with a circuit resistance in the mΩ range. (ii) The magnetic field associated with the thermocurrents can indeed be trapped in the superconductor. Different thermal gradients were applied to the rod resulting in a variation in trapped flux. In order to avoid sources of error in the measurement of the magnetic field, the heaters were always turned off during the superconducting phase transition. Hence, all gradients had to be created by putting the system into a strong thermal disequilibrium before turning off the heaters. The range of achievable gradients was diminished somewhat by this restriction.

The measurement of flux density faced several challenges. For one, the FMs were larger than the cross section dimension of the niobium rod and were designed for use in homogenous fields. Hence, the interpretation of the

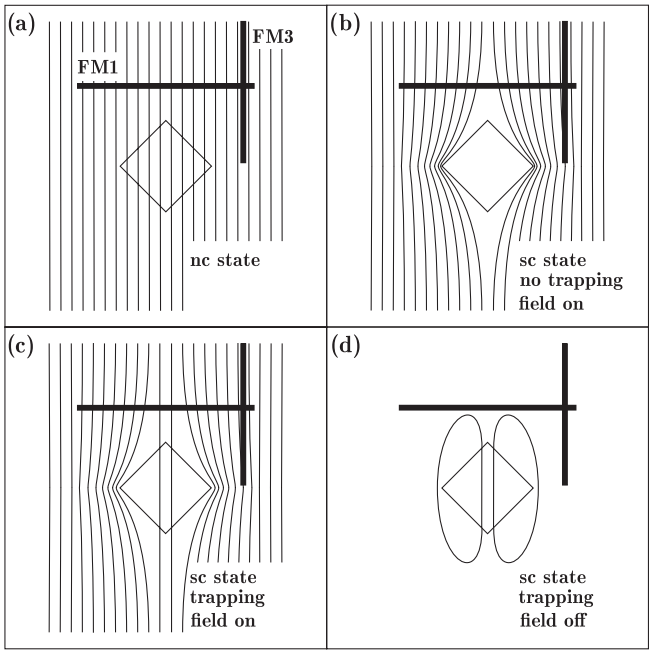

FIG. 8. Orientation of Nb rod, FM1, FM3, and the Helmholtz coil field in the normal-conducting state (a) and after the superconducting phase transition when the rod is in the Meissner state (b). Trapped flux results in an incomplete Meissner effect (c) and can be measured after the external field is turned off (d).

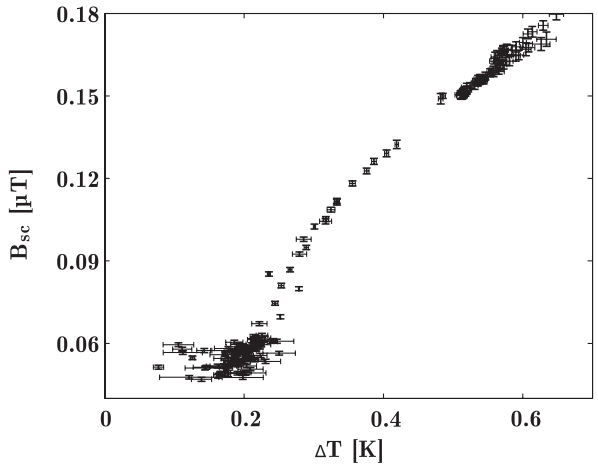

FIG. 9. Trapped magnetic flux in the superconducting sample measured by FM1 as a function of the temperature difference between the two ends of the niobium rod at the instance of phase transition. The phase transition was defined as the instance when the Cernox sensor at the center of the rod fell below the transition temperature.

measured values was challenging. Figure 8(a) shows the orientation of Helmholtz coil field, rod, and the ferromagnetic cores of FM1 and FM3 in the normal-conducting state. The FMs measured the flux density in the direction in which their core was orientated. When the rod was cooled below transition temperature, the FMs registered the variation in flux density due to the Meissner effect [Fig. 8(b)]. The variation was less distinct when the Meissner effect was incomplete and some flux remained pinned in the material [Fig. 8(c)]. In case of 100% flux pinning, the flux distribution and hence the signal would not change. Figure 8(d) displays the field distribution when the external field was turned off after superconducting phase transition. The pinned flux remained trapped in the rod and the FM signal was a measure of the trapped flux in the material. We define the measured signals as described in Table II.

During the experiments concerning the thermoelectric effect, we measured thermocurrents and the associated magnetic field in the normal-conducting state (B_{nc}). The incomplete Meissner effect was observed and the temperature difference along the rod at the instance of superconducting phase transition ΔT was measured by analogy with the cavity measurements. The phase transition was defined as the instance when the Cernox sensor at the center of the rod fell below the transition temperature. Finally, the flux density in superconducting state B_{sc} was acquired after equilibrium ($\Delta T = 0$) was reached. Figure 9 displays the measured value of FM1 versus ΔT. We obtain a distinct correlation. Since all of the ambient field was shielded down below 50 nT, the measured field values of up to 180 nT reveal that an additional field must have been generated and trapped inside the system.

The result is a strong indication for a thermoelectric contribution to R_{res} in SRF cavities. However, the dependency of trapped flux on the temperature difference is assumed to be strongly influenced by the geometry of the setup and can thus not be directly applied to the cavity-tank system. Nevertheless, it should be sufficient for an estimation of the order of magnitude: In the model system a temperature difference of 0.6 K is sufficient to create 0.12 μT additional trapped flux which corresponds to an increase of the surface resistance by 0.4 nΩ in a TESLA-type cavity. Given that the gradients in the cavity-tank system during cooldown were up to 100 times larger, R_{res}

TABLE II. Definition of symbols used in the text.

B_{nc}	Flux density measured in the normal-conducting state [Fig. 8(a)]
B_{sc}	Flux density measured in the superconducting state [Figs. 8(b)–8(d)]
$B_{sc} - B_{nc}$	Calculated "expelled flux" while the applied field remained constant. Difference between Figs. 8(a), 8(b), or 8(c)
$B_{trapped}$	"Trapped flux" [Fig. 8(d)]

variation in the 10 nΩ range, as presented in first section, can reasonably be expected.

2. Meissner effect

Beside the thermoelectric influence on the amount of trapped flux, we studied the impact of temporal gradients. The additional magnetic shielding was removed, increasing the total value of ambient field back to 3 μT (0.3 μT in the FM1 direction). Now, we evaluated the amount of expelled flux ($B_{sc} - B_{nc}$) upon isothermal cooling of the rod, i.e. zero temperature gradient, which could be achieved by adjusting the power of both heaters. We calculated the cooling rate from the slope of the rod's temperature in time. The result is presented in Fig. 10. Note that during isothermal cooling the maximum temperature gradient was always below 0.1 K which, according to Fig. 9, yields no significant flux due to the thermopower.

We observed that the expulsion of an ambient magnetic field due to the Meissner effect was suppressed for high cooling rates (above 40 mK/s) where the rod passed quickly through the transition temperature. For smaller cooling rates (down to 3.6 mK/s) the Meissner effect became more effective. The slower the rod was cooled down, the more flux was expelled and the less flux remained in the rod. This finding is in agreement with earlier published results for a disk-shaped geometry of the sample [5].

Again, the application to a real cavity can only be made qualitatively, since the demagnetization factor influences the driving force of flux expulsion and differs from cavity and rod. Furthermore, we have to point out that all superconducting phase transitions performed with the cavity, especially the cooldown, were not isothermal.

We observed that flux expulsion via Meissner effect (with the Meissner state being energetically more favorable than a state with frozen flux) seems to be more effective when the system remains near T_c for longer periods of time. We tried

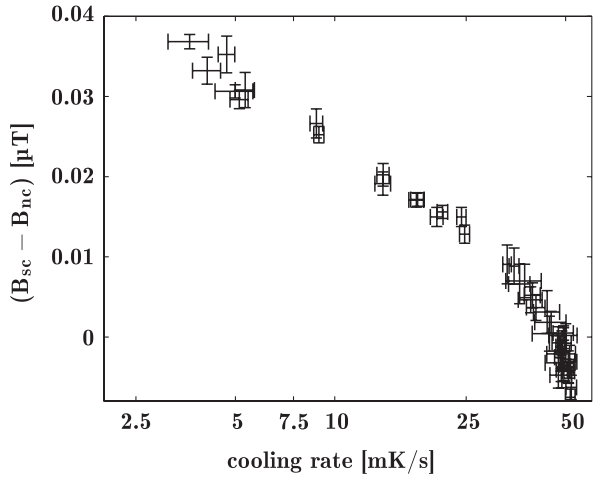

FIG. 10. Expelled flux measured by FM1 versus cooling rate in the model system. B_{nc} during the measurement was 0.3 μT in the FM1 direction and 3 μT in total.

to understand the underlying physics behind this observation by investigating the dynamics of flux expulsion around the superconducting phase transition.

IV. SUMMARY AND CONCLUSION

We have demonstrated an improvement of the residual resistance of an SRF cavity by up to a factor of 2.5 when the cavity was thermally cycled. We believe a temperature gradient along a cavity leads to thermocurrents in the cavity (Nb)—helium tank (Ti)—system. The currents cause magnetic fields which are subsequently trapped in the superconducting material during the phase transition. Thermal cycling to a temperature briefly above T_c diminishes the effects by reducing the temperature gradients prior to the phase transition. This observation may also explain the frequently observed difference in measured Q factors between vertical (no liquid helium tank) and cryomodule tests (helium tank and large temperature gradients). The next steps in our research include the direct observation of thermoelectric voltages and generated fields at the cavity and a detailed simulation of the expected magnetic field close to the cavity's surface.

We were able to gather further evidence for this effect in a model system. In addition, the cooling rate during the superconducting phase transition was found to impact the amount of trapped flux even when the niobium is cooled isothermally. A high cooling rate leads to a suppressed Meissner effect. When the rate is reduced, more flux can be expelled. Both, thermal and spatial gradients, work in the same direction: The larger they are, the higher is the amount of trapped flux and hence the achieved R_{res}. In contrast, a homogenous transition trough T_c leads to a reduction of trapped flux and an improved R_{res} value.

Additional experiments on the model system have shown that the flux trapping behavior is significantly impacted by the cooling dynamics in the temperature range of 9.08 K–T_c. Hence, we need to exercise precise temperature control in that particular temperature regime.

Based on these results we propose to add a step to the standard cavity cooling procedure: The fast cooldown to avoid Q disease should be terminated before the cavity undergoes the superconducting transition, somewhere between 10 and 50 K, and the system should be given time to thermally settle. After achieving a sufficiently uniform temperature distribution, cooling can proceed, ideally in a slow isothermal manner. Alternatively, a short thermal cycle to $\approx$ 20 K should be introduced following the initial rapid cooldown.

ACKNOWLEDGMENTS

We would like to thank Hans-Peter Vogel (RI) for providing the niobium rod and Michael Schuster, Andre Frahm, Sascha Klauke, Dirk Pflückhahn, Stefan Rotterdam, and Axel Hellwig for experimental support.

[1] P. Kneisel, in The 32nd Advanced ICFA Beam Dynamics Workshop on Energy Recovering Linacs (2005) [http://inspirehep.net/record/713900].
[2] B. Bonin and R. Roth, in Proceedings of the 5th Workshop on SRF (1991), p. 210 [http://accelconf.web.cern.ch/AccelConf/SRF91/INDEX.htm].
[3] B. Aune, R. Bandelmann, D. Bloess, B. Bonin, A. Bosotti, M. Champion, C. Crawford, G. Deppe, B. Dwersteg, D. A. Edwards *et al.*, Phys. Rev. ST Accel. Beams **3**, 092001 (2000).
[4] C. Vallet, M. Bolor, B. Bonin, J. P. Charrier, B. Daillant, J. Gratadour, F. Koechlin, and H. Safa, in Proceedings EPAC1992 (1992), p. 1295 [://accelconf.web.cern.ch/AccelConf/e92/Index.htm].
[5] S. Aull, O. Kugeler, and J. Knobloch, Phys. Rev. ST Accel. Beams **15**, 062001 (2012).
[6] A. Gurevich and G. Ciovati, Phys. Rev. B **87**, 054502 (2013).
[7] O. Kugeler, A. Neumann, W. Anders, and J. Knobloch, Rev. Sci. Instrum. **81**, 074701 (2010).
[8] O. Kugeler, W. Anders, A. Neumann, and J. Knobloch, in Proceedings SRF2011 (2011), p. 724 [http://accelconf.web.cern.ch/AccelConf/SRF2011/index.htm].
[9] A. Gurevich, Rev. Accel. Sci. Technol. **5**, 119 (2012) [http://www.worldscientific.com/doi/abs/10.1142/S1793626812300058].
[10] J.-M. Vogt, Master's thesis, Humboldt-Universität zu Berlin, 2013.
[11] J. Milck, Hughes Aircraft Company Technical Report No. AD-750 579, 1970.
[12] F. Primdahl, J. Phys. E **12**, 241 (1979).
[13] Mag01 and Mag01-H, Single Axis Fluxgate Magnetometers, Bartington Instruments (2013).